ACS Symposium on Ordered Fluids and Liquid Crystals, Chicago, Ill., August 1973; (b) see M. J. S. Dewar, A. C. Griffin, and R. M. Riddle, "Liquid Crystals and Ordered Fluids", Vol. 2, J. F. Johnson and R. S. Porter, Ed., Plenum Press, New York, N.Y., 1974, p 733.
(3) M. J. S. Dewar and R. M. Riddle, *J. Am. Chem. Soc.*, **97**, preceding paper (1975).
(4) R. S. Porter, E. M. Barrall II, and J. F. Johnson, *Acc. Chem. Res.*, **2**, 53 (1969).
(5) M. J. S. Dewar and R. S. Goldberg, *J. Am. Chem. Soc.*, **92**, 1582 (1970).
(6) L. Verbit and R. L. Tuggey, *Mol. Cryst. Liq. Cryst.*, **17**, 49 (1972).
(7) L. Verbit and R. L. Tuggey, ref 2b, p 307.
(8) J. T. S. Andrews and W. E. Bacon, *J. Chem. Thermodyn.*, **4**, 515 (1974).
(9) G. W. Gray, "Molecular Structure and the Properties of Liquid Crystals", Academic Press, New York, N.Y., 1962.
(10) S. L. Arora, J. L. Fergason, and T. R. Taylor, *J. Org. Chem.*, **35**, 4055 (1970).
(11) W. R. Young, I. Haller, and D. C. Green, *J. Org. Chem.*, **37**, 3707 (1972).
(12) E. M. Barrall, K. E. Bredfeldt, and M. J. Vogel, *Mol. Cryst. Liq. Cryst.*, **18**, 195 (1972).
(13) M. J. S. Dewar and R. S. Goldberg, *J. Org. Chem.*, **35**, 2711 (1970).
(14) A. De Vries, *Mol. Cryst. Liq. Cryst.*, **10**, 219 (1970).
(15) P. E. Spoerri and A. Erickson, *J. Am. Chem. Soc.*, **60**, 401 (1938).
(16) H. D. Dakin, *Am. Chem. J.*, **42**, 491 (1909).
(17) W. Baker and N. C. Brown, *J. Chem. Soc.*, 2306 (1948).
(18) D. E. Kvalnes, *J. Am. Chem. Soc.*, **56**, 667 (1934).

Circularly Polarized Luminescence and Energy Transfer Studies on Carboxylic Acid Complexes of Europium(III) and Terbium(III) in Solution

Chun Ka Luk and F. S. Richardson*[1]

Contribution from the Department of Chemistry, University of Virginia, Charlottesville, Virginia 22901. *Received November 13, 1974*

Abstract: Circularly polarized luminescence (CPL) and total (unpolarized) luminescence measurements are reported for a number of Eu^{3+} and Tb^{3+} complexes of optically active carboxylic acids in aqueous solution under a variety of physical conditions. Additionally, $Tb^{3+} \rightarrow Eu^{3+}$ energy transfer is studied as a function of pH for aqueous solutions which are 1:5:1 in Tb^{3+}–carboxylic acid–Eu^{3+}. Efficiency of $Tb^{3+} \rightarrow Eu^{3+}$ energy transfer is related to the possible formation of dinuclear or polynuclear complex species either through multiple binding sites on a single carboxylic acid ligand or through ligand + OH^- bridging groups between Tb^{3+}–Eu^{3+} pairs. The results of this study demonstrate the sensitivity of Tb^{3+} and Eu^{3+} CPL to the detailed nature of ligand environment. Changes in ligand type and in donor atom availability (through changes in pH conditions) lead to easily discernible alterations in the sign and intensity patterns of the CPL spectra. Additionally, the extensive splitting of the various ^7F_J multiplet levels of Tb^{3+} and Eu^{3+} due to the low-symmetry ligand fields in Tb^{3+} and Eu^{3+}–carboxylic acid complexes is readily apparent in the CPL spectra, whereas these splittings generally are not resolved in the total luminescence spectra.

I. Introduction

Recently, there has developed considerable interest in the use of the spectroscopic and magnetic properties of lanthanide ions as probes of biomolecular structure and function, particularly for those systems which bind calcium. For example, Birnbaum and Darnall[2-5] have suggested that the visible absorption spectra of lanthanide ions provide a sensitive probe of electrostatic binding sites in proteins and enzymes, and Morallee et al.[6] have emphasized the potential of lanthanide cations as nuclear magnetic resonance probes of biological systems. Additionally, Luk[7] has demonstrated the utility of lanthanide ion emission spectra for characterizing the metal binding sites of a protein (transferrin). More recently, the metal binding sites of several protein structures have been studied by the relatively new spectroscopic emission technique, circularly polarized luminescence (CPL). Gafni and Steinberg[8] have reported the CPL spectra of Tb^{3+} bound to transferrin and to conalbumin, and the CPL of Tb^{3+} bound in a Ca^{2+} site of a carp muscle parvalbumin has been examined in our laboratory.[9]

To better characterize the nature of the lanthanide–ligand linkages in biomolecular systems, a number of recent studies have focused on the structural characteristics of complexes formed by hydroxy- and amino-substituted carboxylic acids with lanthanide ions in aqueous solution. Since it is likely that the lanthanide binding sites of most proteins present $-OH$, $-NH_2$, or $-COO^-$ as ligating groups, it might be expected that carboxylic and amino acid complexes can provide appropriate model systems for studying Ln^{3+}–protein interactions. Katzin and coworkers[10-12] have carried out extensive studies on the circular dichroic properties of Pr^{3+} and Eu^{3+} complexes of α-amino acids and of many hydroxy-substituted carboxylic acids. The circular dichroism (CD) spectra of these systems are highly structured in the region of the metal ion f $\leftrightarrow$ f transitions and are comprised of many more components or bands than the corresponding absorption spectra, reflecting the low-symmetry environment of the metal ion in these complexes. Katzin's studies also revealed that the CD spectra are extraordinarily sensitive to pH changes, suggesting that CD provides a sensitive measure of ligand binding modes in cases where the ligands have several potential donor groups with different pK_a's in aqueous solution. More recently, Martin and coworkers[13] have examined the titration and CD behavior of 12 trivalent lanthanide ions and 15 amino acid ligands in aqueous solution. They noted that although the amino acids form only weak complexes with Ln^{3+} ions, the CD signatures associated with f $\leftrightarrow$ f transitions are very sensitive to the detailed chemical nature of the ligand environment. Furthermore, they concluded from their titration studies that in basic solution the complexes tend to form polynuclear species making the interpretation of the CD data in terms of specific spectra–structure relationships somewhat difficult. Polynuclear complex formation and the simultaneous occurrence of several complex species are problems commonly encountered in solution studies of Ln^{3+} complexes.

Birnbaum and Darnall[14] used difference absorption spectroscopy to study the interaction of Nd^{3+} with acetate, alanine, histidine, benzoate, and anthranilate ligands in aque-

ous solutions under various pH conditions. They found this technique useful in detecting coordination of functional groups of polyfunctional ligands as a function of solution pH. However, they also found that the shapes of the difference spectra are very similar for the Nd^{3+} complexes which have single carboxyl ligands, carboxyl and amino ligands, carboxyl and imidazole ligands, or carboxyl, amino, and imidazole ligands. This suggests that difference absorption spectroscopy may be of limited value for determining the chemical identity or structural details of the binding sites in proteins.

In the study reported here, the structural features of Tb^{3+} and Eu^{3+} complexes of various carboxylic acids were investigated using steady-state luminescence techniques. Both CPL and total luminescence measurements were made under a variety of physical conditions. In addition to varying solution pH and ligand–metal concentration ratios, experiments were carried out in which both Eu^{3+} and Tb^{3+} were present. In these experiments the efficiency of energy transfer between Tb^{3+} and Eu^{3+} was examined. As a working hypothesis, it was assumed that the efficiency of $Tb^{3+} \rightarrow Eu^{3+}$ energy transfer is directly related to the formation of dinuclear or polynuclear complexes in which the two ions may exist in close and rigid contact. Although the central focus of this study is on the structural nature of lanthanide ion–carboxylic acid complexes in aqueous solution, the circularly polarized luminescence data are of some additional and general interest due to the relative novelty of CPL spectroscopy as a molecular structure probe.

II. Circularly Polarized Luminescence (CPL)

In the past 7 years several accounts of CPL experiments and theory have appeared in the literature. Oosterhoff and coworkers[15-17] have reported CPL studies on trans-β-hydrindanone, trans-β-thiohydrindanone, and $(ED)_3Cr(III)\cdot(ClO_4)_3$ in solution (ED is ethylenediamine). Steinberg and coworkers[8,18-21] have reported the CPL spectra of a number of molecules ranging in complexity from 1,1′-bianthracene-2,2′-dicarboxylic acid to several enzyme and metalloenzyme systems. The CPL spectra of camphorquinone and of several Tb^{3+} complexes have been reported recently from our laboratory.[22,23] Furthermore, Snir and Schellman[24] have considered the theory of CPL from molecular systems, giving special attention to how photoselection processes and rotary Brownian motion might be expected to influence the CPL observables.

In the basic CPL experiment, the sample is irradiated with unpolarized light and the radiation emitted by the sample is collected and analyzed for circular polarization as a function of wavelength. In principle, CPL should provide structural information about the emitting states of molecules analogous to that obtained on molecular ground states from CD spectra. For a collection of dissymmetric molecules of random orientation, the sign and intensity of the CD associated with an electronic transition a $\rightarrow$ b are determined by the rotatory strength, $R_{a\rightarrow b}$, of the transition:

$$R_{a\rightarrow b} = \mathrm{Im}\langle\psi_a|\hat{\mu}|\psi_b\rangle \cdot \langle\psi_b|\hat{\mathbf{m}}|\psi_a\rangle \qquad (1)$$

where $\hat{\mu}$ and $\hat{\mathbf{m}}$ are the electric dipole and magnetic dipole operators, respectively. The absorption intensity of this transition is determined in large part by the magnitude of the dipole strength, $D_{a\rightarrow b}$, defined as:

$$D_{a\rightarrow b} = |\langle\psi_a|\hat{\mu}|\psi_b\rangle|^2 \qquad (2)$$

The dissymmetry factor associated with the a $\rightarrow$ b absorptive transition can be defined in terms of the theoretical quantities, $R_{a\rightarrow b}$ and $D_{a\rightarrow b}$, as follows:

$$G(a \rightarrow b) = 4R_{a\rightarrow b}/D_{a\rightarrow b} \qquad (3)$$

This quantity is related to the experimental observables, $\Delta\epsilon$ and ϵ, by the expression:

$$G(a \rightarrow b) = \int_{a\rightarrow b} \Delta\epsilon(\nu)\nu^{-1}d\nu / \epsilon(\nu)\nu^{-1}d\nu \qquad (4)$$

where the integrations are taken over all frequencies spanned by the vibronic manifold of the a $\rightarrow$ b electronic transition, $\Delta\epsilon = \epsilon_L - \epsilon_R$, $\epsilon = (\epsilon_L + \epsilon_R)/2$, and ϵ_L and ϵ_R are respectively the molar extinction coefficients for left- and right-circularly polarized light. It is also useful to provide an operational definition of the absorption dissymmetry factor which is applicable at any given spectral frequency,

$$g(\mathrm{abs}) = \Delta\epsilon/\epsilon \qquad (5)$$

Within the Born–Oppenheimer and Franck-Condon approximations of molecular electronic structure and transitions, the wave functions appearing in the matrix elements of eq. 1 and 2 are determined by the structural or stereochemical characteristics of the molecular ground state. That is, the nuclear configuration of state ψ_b is assumed to be identical with the equilibrium nuclear configuration of state ψ_a. In writing eq. 1 and 2 we take ψ_a and ψ_b to be eigenfunctions of the electronic Schrödinger equation,

$$H(r,Q_a^0)\psi_i = E_i\psi_i \qquad (6)$$

where the nuclei are assumed to be frozen in the equilibrium geometry of the molecular ground state a, represented by the collection of nuclear coordinates Q_a^0. The symbol r denotes the collection of electron coordinates.

If the transition a $\leftarrow$ b displays spontaneous emission, then CPL observations are possible. The sign and intensity of the CPL associated with this transition are gauged by the rotatory strength,[17]

$$R_{a\leftarrow b} = \mathrm{Im}\langle\psi_a|\hat{\mu}|\psi_b\rangle \cdot \langle\psi_b|\mathbf{m}|\psi_a'\rangle \qquad (7)$$

and the intensity of the total luminescence is governed to a good approximation by the dipole strength,

$$D_{a\leftarrow b} = |\langle\psi_a|\mu|\psi_b'\rangle|^2 \qquad (8)$$

The wave functions appearing in eq. 7 and 8 are taken as eigenfunctions of the electronic Schrödinger equation:

$$H(r,Q_b')\psi_i' = E_i'\psi_i' \qquad (9)$$

where the nuclei are assumed to be frozen in the geometrical configuration of the molecular excited state b at the instant of spontaneous emission. If the molecular geometries of the ground state a and the emitting state b are identical at the times of absorption and emission, respectively (i.e., if $\{Q_a^0\} = \{Q_b'\}$), then $R_{a\rightarrow b} = R_{a\leftarrow b}$ and $D_{a\rightarrow b} = D_{a\leftarrow b}$.

The dissymmetry factor associated with the a $\leftarrow$ b emission process may be defined by,

$$G(a \leftarrow b) = 4R_{a\leftarrow b}/D_{a\leftarrow b} \qquad (10)$$

and is related to the observables ΔI and I according to,

$$G(a \leftarrow b) = \int_{a\leftarrow b} \Delta I(\nu)\nu^{-4}d\nu \Big/ \int_{a\leftarrow b} I(\nu)\nu^{-4}d\nu \qquad (11)$$

where the integrations are over all frequencies spanned by the vibronic manifold of the a $\leftarrow$ b electronic transition. As in the case of absorption, it is useful to introduce an operational definition of the luminescence dissymmetry factor which is applicable at specific spectral frequencies:

$$g(\mathrm{lum}) = \Delta I/I \qquad (12)$$

The quantities g(abs) and g(lum) have no theoretical significance in the absence of a detailed model of CD and CPL band shapes. Such a model for CPL requires explicit con-

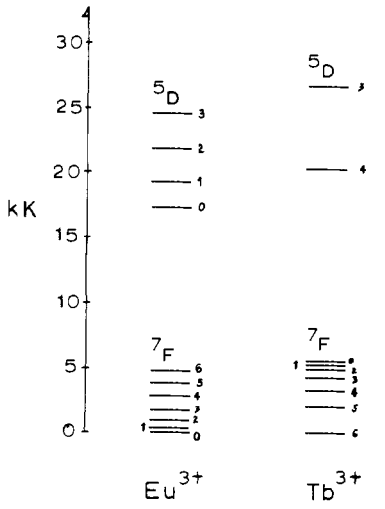

Figure 1. Energy level diagram for Tb(III) and Eu(III) in their free ion forms.

Table I. Transition Energy Assignments for $Eu^{3+}(^5D_0) \leftrightarrow {}^7F_J$ and $Tb^{3+}(^5D_4) \leftrightarrow {}^7F_J$ Transitions[a]

State	ΔE, cm^{-1} [b]	ΔE, cm^{-1} [c]
	$Eu^{3+}(^5D_0) \leftrightarrow {}^7F_J$	
$^7F_0$	17267	17277
$^7F_1$	16887	16917
$^7F_2$	16222	16257
$^7F_3$	15385	15390
$^7F_4$	14390	14412
$^7F_5$	13358	13369
$^7F_6$	12289	12297
	$Tb^{3+}(^5D_4) \leftrightarrow {}^7F_J$	
$^7F_0$	14754	14800
$^7F_1$	14982	15060
$^7F_2$	15430	15462
$^7F_3$	16106	16100
$^7F_4$	17098	17144
$^7F_5$	18350	18400
$^7F_6$	20369	20500

[a] See ref 25. [b] Determined in crystalline $LaCl_3$. [c] Determined in dilute (0.2 *M*) $HClO_4$ solution at 25°C.

sideration of vibrational-electronic interactions, Franck-Condon overlap factors, solute-solvent interactions, and competitive processes involving electronic and vibrational relaxation from Franck-Condon excited states.

The preceding discussion regarding the rotatory strength of luminescent molecular transitions applies rigorously only in those cases where the emitting molecules are randomly oriented and the equilibration time for rotary molecular motion is short compared to the radiative lifetime of the emitting states. If these latter conditions are not fulfilled, then the expressions for rotatory strength and dissymmetry factors must be modified to reflect any macroscopic anisotropy in the emitting sample.[24]

As is apparent from eq 1, 6, 7, and 9, CPL provides a spectroscopic probe of molecular emitting states which is analogous to the CD probe utilized with extraordinary success in studying the stereochemical and electronic structural features of dissymmetric molecules in their ground states.

In the present application of CPL to the study of lanthanide ion complexes in solution, we measure the emission associated with metal ion f ↔ f transitions. It is generally assumed that the f electrons in these systems interact only weakly with the ligand and solvent environment and that the structural (i.e., stereochemical) properties of the f-f excited states should not differ significantly from those of the electronic ground state. Comparisons of g(abs) and g(lum) at a number of frequencies in the region of the $^7F_6 \leftrightarrow {}^5D_4$ Tb^{3+} transition in several Tb^{3+}-carboxylic acid complexes suggest that $G(^7F_6 \leftarrow {}^5D_4) \sim G(^7F_6 \rightarrow {}^5D_4)$ for these systems.[22] In this case, CD and CPL may yield similar and possibly redundant information. However, CPL has significant advantages over CD in the study of systems whose transitions are very weak (such as the f ↔ f transitions of lanthanide ions) or which have low-lying electronic excited states inaccessible to conventional absorption techniques (such as the various multiplet components split out of the ground configurational states of many lanthanide ions). Whereas the absorption and CD intensities of the lanthanide f ↔ f transitions generally require operating near the sensitivity limits of most absorption/CD spectrophotometers, the emission and CPL intensities generally are easily detectable even when small concentrations of the luminescent molecules are required or desired. Additionally, the multiplet components, split out of the ground configurational states of ion such as Tb^{3+} and Eu^{3+}, are connected to the excited configurational states of these systems by radiative transitions which are readily observed in the visible and near ir luminescence and CPL spectra.

III. Energy Levels and Electronic States of Tb(III) and Eu(III)

Energy level diagrams for Tb(III) and Eu(III) in their free ion forms are shown in Figure 1. Transition energy assignments for transitions between the lowest lying level of the first excited-term multiplet (^5D) and the various levels of the ground-term multiplet (^7F) in both Tb^{3+} and Eu^{3+} are listed in Table I. In aqueous solution, the $^5D_0$ level of Eu^{3+} lies approximately 3220 cm^{-1} below the $^5D_4$ level of Tb^{3+}. Thus, in a mixed solution containing both Eu^{3+} and Tb^{3+} ions, it is possible that the energy transfer process,

$$Tb^{3+}(^5D_4) + Eu^{3+}(^7F_J) \rightarrow Tb^{3+}(^7F_J) + Eu^{3+}(^5D_0)$$

may occur. If $Tb^{3+}(^5D_4)$ is an emitting species in the absence of Eu^{3+} ions, it is likely that its emission will be partially quenched in the presence of Eu^{3+} ions due to competition between the radiative process (emission) and the $Tb^{3+} \rightarrow Eu^{3+}$ energy transfer process.

The rotatory strengths associated with the transitions $^5D_J \rightarrow {}^7F_J$ in Eu^{3+} and Tb^{3+} depend upon the magnitudes and relative orientations of the corresponding electric and magnetic transition dipoles. Nonvanishing rotatory strengths arise only when the electric and magnetic transition dipoles are nonorthogonal. The degree to which these transition dipoles are nonorthogonal is determined entirely by those components of the ligand field potential which are dissymmetric (i.e., lacking an alternating rotation-reflection axis of any order). The *magnitudes* of the transition dipoles (independent of their orientations) will also be influenced by these low-symmetry ligand-field components, but generally the spherical symmetry of the free ion and the high-symmetry components of the ligand field will dominate the selection rules and determine the magnitudes of the transition dipoles. For the $^5D_J \rightarrow {}^7F_J$ transitions of Eu^{3+} and Tb^{3+}, the dominant selection rule for magnetic dipole processes is $\Delta J = 0, \pm 1$, except for $J = 0 \rightarrow J = 0$. Ligand-field mixing or vibronically induced mixing of J states may produce weak magnetic dipole transitions with $\Delta J \geq 2$, but the $\Delta J = 0, \pm 1$ rule is generally satisfied.

The only restriction on ΔJ governing electric dipole transitions between different J states is $\Delta J \leq 6$, although transitions from J = even to J = odd states are usually weak in ions with an even number of electrons in the f shell (as in

Eu^{3+}, f^6, and in Tb^{3+}, f^8). This statement assumes, of course, that an effective mechanism exists for mixing states of opposite parities or scrambling the f orbitals with orbitals which are ungerade with respect to inversion. Ungerade ligand field components or vibronic coupling via ungerade vibrational modes provides such a mechanism. Dissymmetric complexes will always possess ligand fields which have both gerade and ungerade components.

In light of the selection rules discussed above, we may expect that the $^5D_0 \rightarrow {}^7F_1$ transition will be the most optically active (largest rotatory strength) among the $^5D_0 \rightarrow {}^7F_J$ transitions of Eu^{3+}. Among the $^5D_4 \rightarrow {}^7F_J$ transitions of Tb^{3+}, we may expect the $^5D_4 \rightarrow {}^7F_5$, $^7F_4$, and $^7F_3$ transitions to exhibit the largest rotatory strengths. These predictions are based on magnetic dipole selection rules only, and completely neglect considerations of relative electric dipole strengths and electric dipole-magnetic dipole orientation factors.

IV. Experimental Section

A. Spectroscopic Measurements. The luminescence experiments were carried out using a high-sensitivity emission spectrophotometer in which emission is detected in a direction 90° to the direction of excitation. The light source was a 750 W high-pressure Hg-Xe arc lamp. Both the excitation and emission monochromators were Spex Model 1670 grating instruments fitted with gratings blazed at 5000 Å. The scattered light level of these monochromators is <0.05%. In all the experiments reported here an excitation bandwidth of 100 Å and an emission bandwidth of 10 Å were used. The excitation beam was mechanically chopped at a frequency of 13 Hz and the emission beam was passed through an optical phase modulator (modulation frequency 50 kHz) immediately following its exit from the sample cell. The phase modulator (manufactured by Morvue, Tigard, Oregon) in conjunction with a linear polarizing element serves as an analyzer for the circularly polarized components of the emitted radiation. The 50-kHz component of the ac optical signal arriving at the detector is alternately proportional to the intensities of the left and right circularly polarized components of the sample luminescence.

The detector was a Centronics Q42835 photomultiplier of the trialkali extended-red type, housed in a photomultiplier cooler (Model TE104TS, Products for Research, Inc.) to minimize dark current. The electrical signal at the detector consists of a large ac component of frequency 13 Hz which is proportional to total emission intensity (independent of state of polarization), plus a smaller ac component of frequency 50 kHz whose magnitude and phase carry the CPL intensity and sign variables. This signal is processed by two lock-in amplifiers operating in parallel and tuned at 13 Hz and 50 kHz, respectively. The total emission (luminescence) and CPL spectra are recorded simultaneously by a two-pen strip-chart recorder (Speedomax XL Recorder, Leeds and Northrup).

Two quantities are measured directly in our luminescence experiments, total emission intensity (I) and the difference in intensities of the left and right circularly polarized components of the emitted radiation ($\Delta I = I_L - I_R$). We do not measure absolute emission intensities, so I and ΔI are given in relative quantal units and the ratio $(\Delta I/I) = g(\text{lum})$ is the only quantity for which we obtain absolute values. Calibration of our instrumentation to obtain absolute values (signs and magnitudes) of g(lum) was carried out using a procedure previously described by Steinberg and Gafni.[19]

The CD spectra reported here were obtained with a Durrum-Jasco J10B CD/MCD spectrophotometer interfaced with a Spex Model 1400 II ¾ meter grating double monochromator. The uv-vis absorption spectra were obtained on a Cary 14R spectrophotometer.

All the spectroscopic measurements were performed at room temperature. In the emission experiments, an existing wavelength of 3650 Å ($\Delta\lambda_{exc}$ = 100 Å) was used when exciting Tb^{3+} ions, and 3910 Å ($\Delta\lambda_{exc}$ = 100 Å) was used for exciting Eu^{3+} ions.

B. Samples. The ligands employed in this study were: (1) L-malic acid (L-Mal); (2) L-aspartic acid (L-Asp); (3) L-glutamic acid (L-Glu); (4) L-serine (L-Ser); (5) L-alanine (L-Ala); and, (6) L-lactic acid (L-Lac). All experiments were performed on samples prepared by mixing aqueous solutions of these carboxylic acid compounds with aqueous solutions of $TbCl_3$, $EuCl_3$, or $TbCl_3$ + $EuCl_3$. The $LnCl_3$ solutions were prepared by dissolving 99.9% pure metal oxides (Eu_2O_3, Tb_2O_3) in HCl. Adjustments of sample pH were done with 6 *M* NaOH or 9 *M* NH_3. Ligand-metal concentration ratios ([L]/[M]) were varied from experiment to experiment and are noted along with the spectral results which are presented.

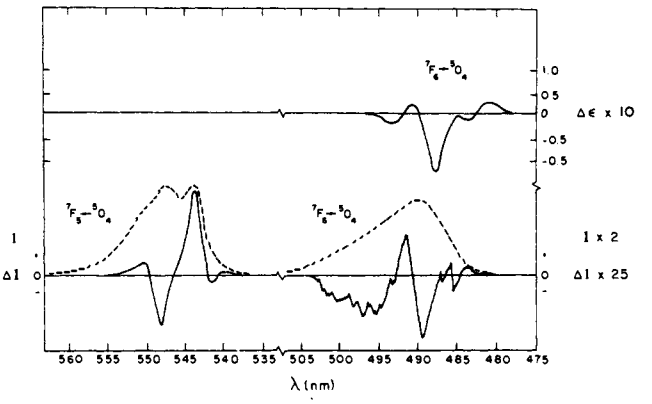

Figure 2. CD (upper solid curve), CPL (lower solid curve), and total luminescence (lower dashed curve) spectra for 1:5 Tb^{3+}-L-malic acid in solution at pH 8.54. (Note different ΔI and I scales for the two transition regions, $^7F_5 \leftarrow {}^5D_4$ and $^7F_6 \leftarrow {}^5D_4$.) g(lum) = 0.080($\Delta I/I$).

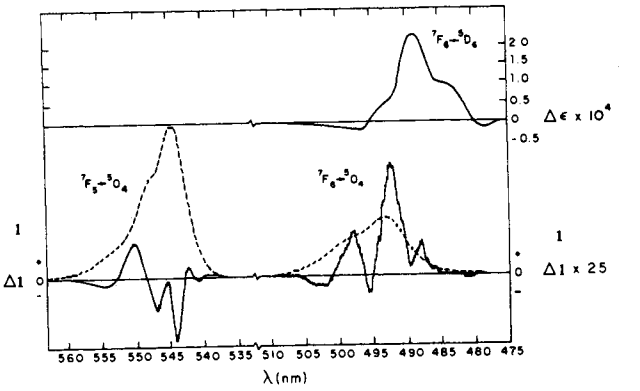

Figure 3. CD (upper solid curve), CPL (lower solid curve), and total luminescence (lower dashed curve) spectra for 1:5 Tb^{3+}-L-aspartic acid in solution at pH 8.54. (Note different ΔI scales for the two transition regions, $^7F_5 \leftarrow {}^5D_4$ and $^7F_6 \leftarrow {}^5D_4$.) g(lum) = 0.200($\Delta I/I$).

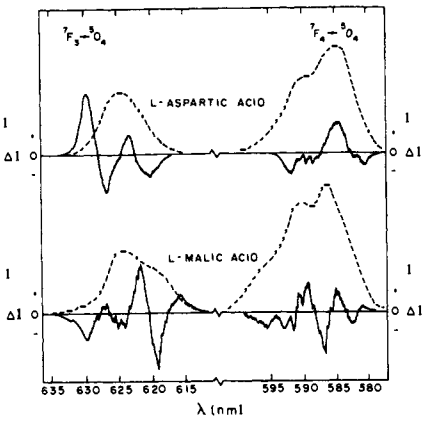

Figure 4. CPL (solid curves) and total luminescence (dashed curves) spectra of 1:5 Tb^{3+}-L-malic acid and Tb^{3+}-L-aspartic acid in solution at pH 8.54. g(lum) = 0.040 ($\Delta I/I$).

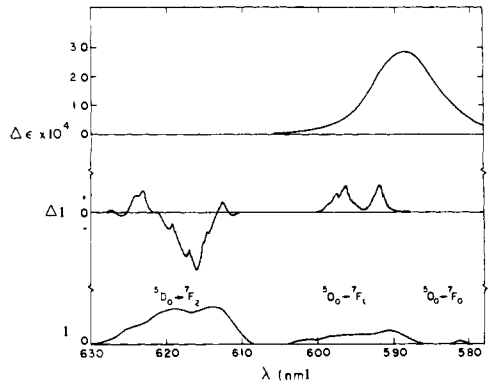

Figure 5. CD, CPL, and total luminescence spectra for 1:5 Eu^{3+}-L-malic acid in solution at pH 8.64. $g(\text{lum}) = 0.001(\Delta I/I)$.

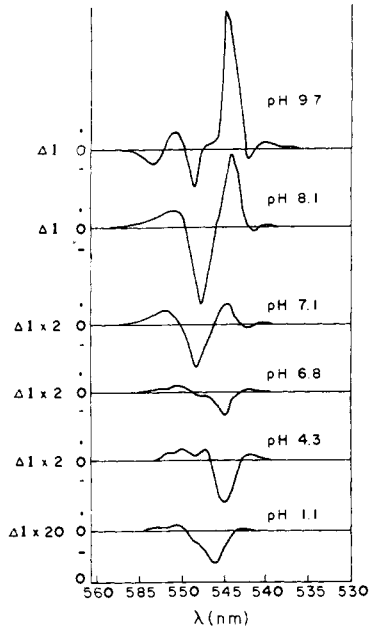

Figure 6. CPL spectra of 1:5 Tb^{3+}-L-malic acid in the region of the $Tb^{3+}(^7F_5) \leftarrow {}^5D_4$ transition for various values of solution pH. $g(\text{lum}) = 0.160\ (\Delta I/I)$, where I can be obtained directly from Figure 7.

V. Results

The CD, CPL, and total luminescence spectra associated with the $^7F_6 \leftrightarrow {}^5D_4$ and $^7F_5 \leftarrow {}^5D_4$ transitions of Tb^{3+} in a 5:1 L-Mal-Tb^{3+} solution at pH 8.54 are displayed in Figure 2. A similar set of spectra for a 5:1 L-Asp-Tb^{3+} solution at pH 8.54 are shown in Figure 3. In Figure 4 are displayed the CPL and total luminescence spectra arising from the $^7F_4 \leftarrow {}^5D_4$ and $^7F_3 \leftarrow {}^5D_4$ transitions of Tb^{3+} in 5:1 L-Mal-Tb^{3+} and 5:1 L-Asp-Tb^{3+} solutions at pH 8.54.

The $g(\text{lum}) = \Delta I/I$ and $g(\text{abs}) = \Delta\epsilon/\epsilon$ values in the $^7F_6 \leftrightarrow {}^5D_4$ region for both the L-Mal and L-Asp complexes of Tb^{3+} have the same signs and nearly the same magnitudes, indicating similar ground state and emitting state geometries. Among the $^7F_{6,5,4,3} \leftarrow {}^5D_4$ transitions of Tb^{3+} (in solution with L-Mal and with L-Asp), the $g(\text{lum})$ values throughout the $^7F_5, ^7F_3 \leftarrow {}^5D_4$ transition regions are about an order of magnitude larger than the $g(\text{lum})$ values observed in the $^7F_6, ^7F_4 \leftarrow {}^5D_4$ transition regions (see Table I of ref 22). The $g(\text{lum})$ values at frequencies corresponding to extrema in the CPL spectra of the $^7F_{6,5,4,3} \leftarrow {}^5D_4$ Tb^{3+} transitions range from $\sim 10^{-1}$ to $\sim 10^{-3}$ for solutions which are 5:1 in ligand (L-Mal or L-Asp)-Tb^{3+} molar concentration ratios and are at pH 8.54.

L-Mal and L-Asp differ only with respect to substitution at the α carbon. L-Mal has a hydroxyl group and L-Asp has an amino group attached to the α carbon. At pH 8.54, both carboxyl moieties of L-Mal and of L-Asp are deprotonated and presumably provide strong donor groups for coordination to Tb^{3+}. Structural differences between Tb^{3+}-L-Mal and Tb^{3+}-L-Asp can be attributed, therefore, to differences between the -OH and $-NH_2$ moieties as potential donor groups (thus making the ligands terdentate rather than bidentate *or* promoting dinuclear or polynuclear complex formation) or as vicinal perturbing groups which can indirectly influence the structural details of the inner coordination sphere (donor atoms bound directly to the metal ion). CD and CPL are expected to be quite sensitive to such structural features and the spectra shown in Figures 2, 3, and 4 strongly suggest considerable structural differences between the Tb^{3+}-L-Mal and Tb^{3+}-L-Asp complexes existing in aqueous solution at pH 8.54.

The CPL and total luminescence spectra of Tb^{3+}-L-Glu at pH 8.54 are similar to those reported here for Tb^{3+}-L-Asp. The CPL intensities for the Tb^{3+}-L-Glu complex are slightly less (~20%) than those observed for the Tb^{3+}-L-Asp complex; L-Glu differs from L-Asp by just one $>CH_2$ unit in the hydrocarbon chain so that one would not expect much difference in their coordination properties unless chelate ring size is a critical factor. L-Glu will form eight-membered chelate rings if it is bidentate through its $-COO^-$ groups, whereas L-Asp will form seven-membered chelate rings if it is bidentate through its $-COO^-$ groups.

The CPL and total luminescence spectra associated with the $^7F_0, ^7F_1, ^7F_2 \leftarrow {}^5D_0$ transitions of Eu^{3+} in a 5:1 L-Mal-Eu^{3+} solution at pH 8.64 are shown in Figure 5. Also displayed in Figure 5 is the CD spectrum of this 5:1 L-Mal-Eu^{3+} system in the 610–580 nm spectral region. $\Delta\epsilon_{max}$ (λ = 589 nm) = 2.8×10^{-4}/mol of Eu^{3+} and g_{589} (abs) = 2.4×10^{-3} for this complex, and the observed $g(\text{lum})$ values at selected wavelengths are:

λ, nm	$g(\text{lum}) \times 10^3$	
592	2.4	$^7F_1 \leftarrow {}^5D_0$
597	2.6	$^7F_1$
616	−1.7	$^7F_2$
624	1.0	$^7F_2$

Note that the dissymmetry factors in the region of the magnetic dipole allowed $^7F_1 \leftarrow {}^5D_0$ transition are larger than those in the region of the magnetic dipole forbidden $^7F_2 \leftarrow {}^5D_0$ transition. These selection rules are not expected to be particularly strong in complexes of the type considered here since the ligand-field symmetries are quite low (as evidenced by the easily observable splittings within multiplet sublevels) and ligand-field induced J-level mixings are expected to be substantial.

The pH dependence of Tb^{3+} emission (CPL and total luminescence) in the $^7F_5 \leftarrow {}^5D_4$ transition region is demonstrated by the spectra shown in Figures 6–10. In the case of Tb^{3+}-L-Mal, not only do CPL intensities (that is, peak intensities, *not* net or total intensities) increase as pH is increased, but the qualitative shape and sign pattern of the CPL signature changes as pH is varied. This provides strong evidence of significant structural alterations in the complex species as pH is varied. The pH dependence of the band shapes and intensities observed in the total luminescence spectra of Tb^{3+}-L-Mal lead to similar conclusions.

The CPL of Tb^{3+}-L-Ser over the pH range 3.0–7.5 changes in intensity but not in sign pattern (see Figure 8). Between pH 7.5 and 10.0 the CPL sign pattern changes, but not in any drastic way. The shape of the total luminescence band for the $^7F_5 \leftarrow {}^5D_4$ transition in this system ap-

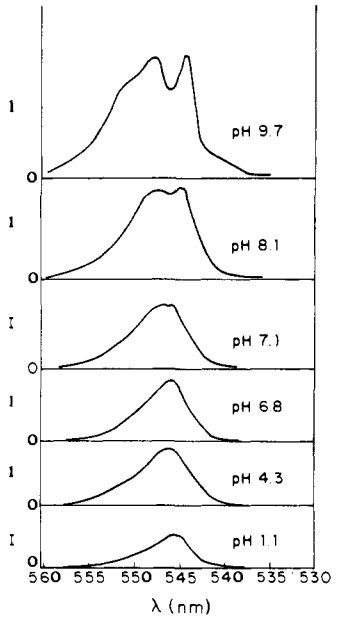

Figure 7. Total luminescence spectra of 1:5 Tb^{3+}-L-malic acid in the region of the $Tb^{3+}(^7F_5) \leftarrow {}^5D_4$ transition for various values of solution pH.

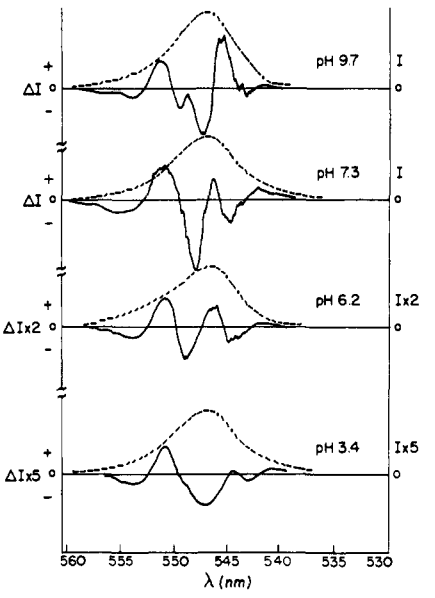

Figure 8. CPL (solid curves) and total luminescence (dashed curves) spectra of 1:5 Tb^{3+}-L-serine in the region of the $Tb^{3+}(^7F_5) \leftarrow {}^5D_4$ transition for various pH values. $g(\text{lum}) = 0.105(\Delta I/I)$.

pears to be independent of pH, although its intensity does increase with increasing pH. Tb^{3+}-L-Ala exhibits no CPL below pH ~6.5. CPL intensity increases with increasing pH over the range of 6.5-9.0, but the sign pattern changes only slightly (see Figure 9).

The CPL and luminescence of Tb^{3+}-L-Lac were measured at just two pH values, 1.12 and 0.46 (see Figure 10). In this case we used a [L]/[M] ratio of 10:1. Precipitation occurs at pH >1.2. We also attempted to get 2-methylpentanoic acid (the simplest optically active aliphatic carboxylic acid) into solution with aqueous $TbCl_3$ and $EuCl_3$, but in each case the metal hydroxide compound precipitated out when base was added.

The ratios of total luminescence intensities for Tb^{3+}-L-Mal, L-Ser, and L-Ala complexes vs. Tb^{3+} (the pure $TbCl_3$) in solution are plotted as functions of pH in Figures 11, 12, and 13. The Tb^{3+} emission from pure $TbCl_3$ in aqueous solution is nearly constant over the pH range in which Tb^{3+} stays in solution. In constructing the plots shown in Figures 11-13, Tb^{3+} emission intensity was taken to be that observed at low pH. It enters as a constant in the ratios appearing in these figures. The Tb^{3+}-ligand solutions were 0.1 *M* in Tb^{3+} and 0.5 *M* in ligand. The $TbCl_3$ solution was 0.1 *M* in Tb^{3+}.

Also shown in Figures 11, 12, and 13 is the extent to which Eu^{3+} ions quench the $^7F_5 \leftarrow {}^5D_4$ Tb^{3+} emission when present in equimolar amounts in an aqueous solution of Tb^{3+}-ligand-Eu^{3+}. The quenching data presented in Figures 11, 12, and 13 were obtained on solutions which were 0.1 *M* in Eu^{3+}, 0.1 *M* in Tb^{3+}, and 0.5 *M* in ligand (L-Mal, L-Ser, or L-Ala). Significantly, quenching of Tb^{3+} emission in the Tb^{3+}-ligand-Eu^{3+} solutions is accompanied by a proportionate enhancement of Eu^{3+} emission. This observation strongly suggests that the quenching of Tb^{3+} emission results from energy transfer to Eu^{3+} ions (followed by Eu^{3+} emission) rather than from displacement of Tb^{3+} ions by Eu^{3+} ions from ligand binding sites. Furthermore, excitation of Tb^{3+} in aqueous solution which is 0.05 *M* in both Tb^{3+} and Eu^{3+} does not lead to observable Tb^{3+} emission quenching-Eu^{3+} emission enhancement over the pH range 1.5-5.0.

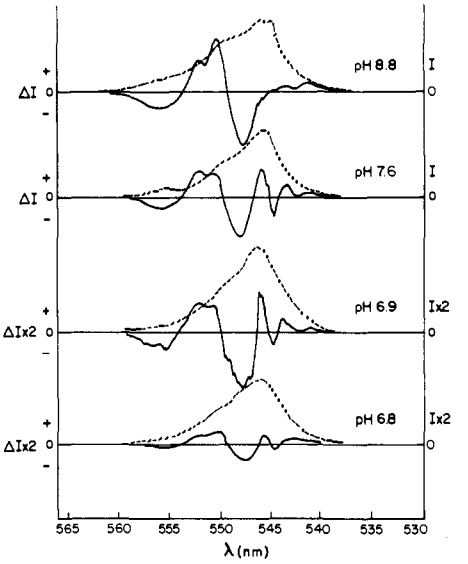

Figure 9. CPL (solid curves) and total luminescence (dashed curves) spectra of 1:5 Tb^{3+}-L-alanine in the region of the $Tb^{3+}(^7F_5) \leftarrow {}^5D_4$ transition for various pH levels. $g(\text{lum}) = 0.133(\Delta I/I)$.

In Figure 14, $\Delta I/[Tb^{3+}]$, measured at 5441.5 Å, is plotted as a function of $[Eu^{3+}]/[Tb^{3+}]$ for aqueous solutions of Tb^{3+}-L-Mal-Eu^{3+} at two different pH values. $g(\text{lum})$ at 5441.5 Å for Tb^{3+}-L-Mal-Eu^{3+} is constant with respect to $[Eu^{3+}]/[Tb^{3+}]$. Furthermore, the qualitative features (sign patterns and relative band intensities) of the Tb^{3+} CPL spectrum in Tb^{3+}-L-Mal-Eu^{3+} remain invariant to $[Eu^{3+}]/[Tb^{3+}]$ in the pH range 1.1-8.5. The Tb^{3+} CPL spectrum in Tb^{3+}-L-Ala-Eu^{3+} is also invariant (except, of course, for intensity reduction) to $[Eu^{3+}]/[Tb^{3+}]$ at pH 7.6, but is not invariant at pH 8.3. In the latter case, nonnegligible alterations occur in the Tb^{3+} CPL signature in the $^7F_5 \leftarrow {}^5D_4$ region (see Figure 15).

Variations in [L-Mal]/[Tb^{3+}] from 20:1 to 4:1 do not result in any qualitative (and only very slight quantitative) changes in the CPL spectrum of Tb^{3+} at pH 8.2 and 4.4.

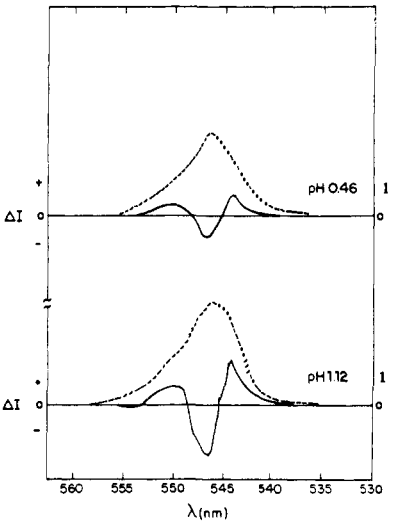

Figure 10. CPL (solid curves) and total luminescence (dashed curves) spectra of 1:10 Tb^{3+}-L-lactic acid in the region of the $Tb^{3+}(^7F_5) \leftarrow {}^5D_4$ transition at two pH values. $g(\text{lum}) = 0.021(\Delta I/I)$.

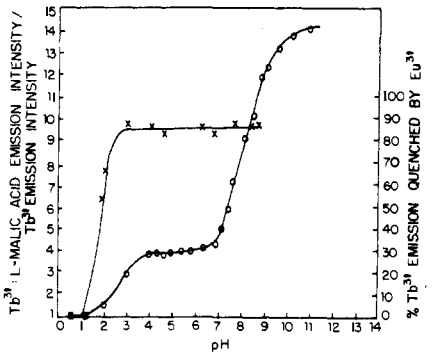

Figure 11. pH dependence of Tb^{3+}-L-malic acid emission intensity/Tb^{3+} ($TbCl_3$ in solution at low pH) emission intensity (O) and of % Tb^{3+} luminescence quenched by Eu^{3+} in a solution of 1:5:1 Tb^{3+}-L-malic acid-Eu^{3+} (×). The intensities used in determining these data were total integrated intensities (band areas *not* peak heights) observed for $Tb^{3+}(^7F_5) \leftarrow {}^5D_4$ emission.

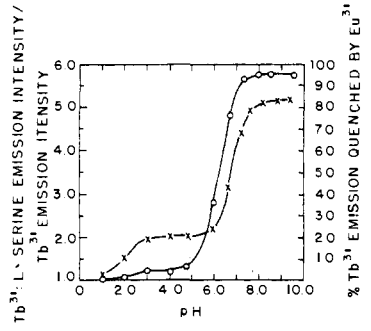

Figure 12. pH dependence of Tb^{3+}-L-serine emission intensity/Tb^{3+} ($TbCl_3$ in solution at low pH) emission intensity (O) and of % Tb^{3+} luminescence quenched by Eu^{3+} in a solution of 1:5:1 Tb^{3+}-L-serine-Eu^{3+} (×). Total integrated intensities (band areas *not* peak heights) of the $^7F_5 \leftarrow {}^5D_4(Tb^{3+})$ emission were used to obtain these data.

VI. Discussion

The spectra shown in Figures 2-4, 6, and 8-10 demonstrate the sensitivity of Tb^{3+} CPL to the detailed nature of ligand environment. Changes in ligand type and in donor atom availability (through changes in pH conditions) lead

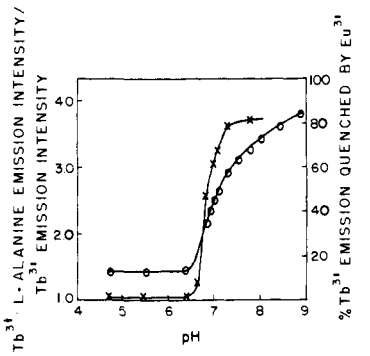

Figure 13. pH dependence of Tb^{3+}-L-alanine emission intensity/Tb^{3+} ($TbCl_3$ in solution at low pH) emission intensity (O) and of % of Tb^{3+} luminescence quenched by Eu^{3+} in a solution of 1:5:1 Tb^{3+}-L-alanine-Eu^{3+} (×). The intensities used in determining these data were total integrated intensities (band areas) observed for $Tb^{3+}(^7F_5) \leftarrow {}^5D_4$ emission.

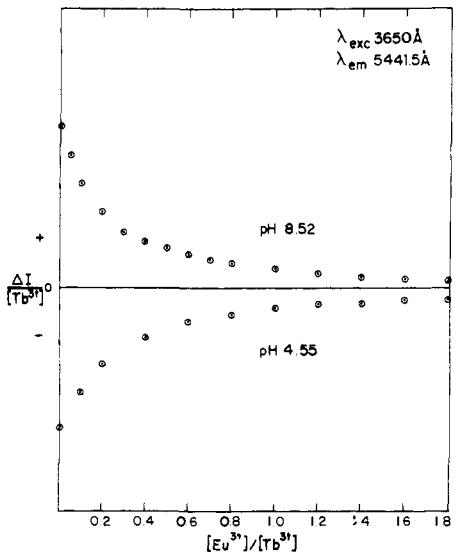

Figure 14. $\Delta I/[Tb^{3+}]$ vs. $[Eu^{3+}]/[Tb^{3+}]$ for Tb^{3+}-L-malic acid-Eu^{3+} in solution at pH 8.52 and at pH 4.55. ΔI was monitored at λ 5441.5, a wavelength at which the CPL of Tb^{3+}-L-malic acid exhibits an extremum.

to easily discernible alterations in the sign patterns and intensity patterns of the CPL spectra. The total luminescence spectra are less sensitive to structural alterations in the ligand environment of Tb^{3+}. Additionally, the extensive splitting of the various ^7F_J multiplet levels due to the low-symmetry ligand fields present in the complexes studied here is readily apparent in the CPL signatures, whereas these splittings generally are not detected in the total luminescence spectra.

The pH dependence of Tb^{3+}-L-Mal luminescence is illustrated by the data shown in Figures 6, 7, and 11. These data were obtained from emission measurements in the region of the $^7F_5 \leftarrow {}^5D_4$ transition of Tb^{3+}. Emission data obtained in the $^7F_6$, $^7F_4$, $^7F_3 \leftarrow {}^5D_4$ transition regions of Tb^{3+}-L-Mal exhibit a similar pH dependence. The sign pattern of the CPL does not change significantly between pH ~1.0 and pH ~6.8. However, the sign pattern is completely altered in the region pH 6.8-7.0, and then remains unchanged throughout the region pH 7.0-9.5. Around pH 9.6, the CPL sign pattern again changes, but only slightly, and then remains unchanged until the onset of precipitation (pH ~ 10.5-11.0). Between pH ~1.0 and pH ~4.0 L-Mal is presumably unidentate ($-COO^-$ donor group); between pH

~4.0 and pH ~6.5, L-Mal may be bidentate through two ionized $-COO^-$ groups and possibly terdentate if the neutral -OH group can also bind; at pH >6.5 L-Mal is most likely terdentate with two $-COO^-$ donor groups and one -OH (or $-O^-$) donor group. It is tempting to attribute the rather small changes in the CPL of Tb^{3+}-L-Mal over the pH range 1.0-6.8 to structural changes in the complex arising from the relative unidentate vs. bidentate proclivities of L-Mal under these pH conditions, and to relate the rather large and abrupt change in CPL near pH 6.8 to the possibly terdentate nature of L-Mal at pH > 6.5. In the unidentate binding mode, only "vicinal effects"[6] originating with the asymmetric center in L-Mal may contribute to the observed chiroptical properties (in this case, ΔI). In the bidentate binding mode, both "vicinal effects" and chelate ring "conformational dissymmetry" may contribute.[26] In the terdentate binding mode, each bound ligand can contribute "configurational" dissymmetry as well as ring conformation dissymmetry and asymmetric vicinal groups.[26] It is reasonable to expect then that a change from unidentate or bidentate binding to terdentate binding will result in a substantial change in chiroptical observables (intensities and/or sign patterns). This interpretation of the CPL shown in Figure 6 must be offered with some reservation, however, since the extent of Ln^{3+} hydrolysis at pH > 6.5 and the influence of this hydrolysis on the Ln^{3+} spectral properties have not been fully characterized. It is certain that Ln^{3+} hydrolysis begins in the neutral pH range and it seems likely that the spectral properties will be somewhat sensitive to the replacement of H_2O by OH^- in the coordination sphere (see ref 13).

The pH dependence of Tb^{3+}-L-Ser luminescence is illustrated by the data displayed in Figures 8 and 12. These data were obtained from measurements in the region of $^7F_5 \leftarrow {}^5D_4$ Tb^{3+} emission. The pH dependence of Tb^{3+} luminescence in the regions of the transitions, $^7F_6$, $^7F_4$, $^7F_3 \leftarrow {}^5D_4$, is similar to that found in the $^7F_5 \leftarrow {}^5D_4$ region. We note that the sign pattern in the Tb^{3+}-L-Ser CPL signature remains essentially unchanged over the pH range 3.4-9.7, although relative band intensities, band splittings, and frequencies of band maxima change in this pH region. Furthermore, we note that the g(lum) values at several of the wavelengths corresponding to ΔI extrema are constant over the pH range 3.4-9.7. These findings are unlike those noted previously for the Tb^{3+}-L-Mal system under similar conditions.

The potential donor groups of L-Ser are $-COO^-$, -OH (or $-O^-$), and $-NH_2$. Amino groups are very weak ligands for lanthanide ions and generally will not bind when oxygen donor atoms are available. There is a conspicious absence of Ln^{3+}-N type complexes which have been prepared in aqueous solution owing to the inability of most N donors to compete with H_2O for the Ln^{3+} ions. Complexation of a weakly basic N donor could occur only by displacement of strongly bound water molecules. The calculated enthalpy of hydration (−800 to −900 kcal/mol)[27] is indicative of the strength of the Ln^{3+}-OH_2 interaction. Additionally, the large excess of solvent molecules makes it even more difficult for the relatively small number of N donors to compete effectively. Strongly basic N donors, which might otherwise be expected to form strong Ln^{3+}-N bonds, generate a sufficient concentration of hydroxide ion by interaction with water to precipitate the highly insoluble lanthanide hydroxides.

In view of the relatively weak affinity of Ln^{3+} ions for N donors, especially in aqueous solution, it seems unlikely that L-Ser will be terdentate through $-COO^-$, -OH, and $-NH_2$ to Ln^{3+} in solution. It is quite probable, however, that L-Ser will be bidentate through the carboxylate and hydroxyl groups. The data shown in Figures 8 and 12 can be interpreted in terms of unidentate L-Ser binding between pH ~1 and pH ~6 and bidentate L-Ser binding at pH >6.0. Again it must be noted that Ln^{3+} hydrolysis beginning in the neutral pH region is expected and that this may also influence the spectroscopic observables, ΔI and I. The g(lum) values observed at various ΔI and I extrema are of similar magnitudes in the emission spectra of Tb^{3+}-L-Mal and Tb^{3+}-L-Ser. However, between pH ~ 3.5 and ~10 the values of both I and $|\Delta I|$ (at extrema in the total luminescence and CPL spectra) are about three times greater for Tb^{3+}-L-Mal than for Tb^{3+}-L-Ser.

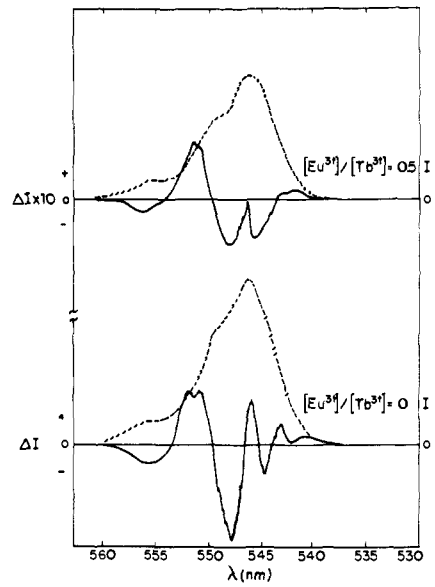

Figure 15. CPL (solid curves) and total luminescence (dashed curves) spectra of 1:5 Tb^{3+}-L-alanine (lower spectra) and of 2:10:1 Tb^{3+}-L-alanine-Eu^{3+} (upper spectra) in solution at pH 8.3. g(lum) = $0.133(\Delta I/I)$.

The pH dependence of Tb^{3+}-L-Ala luminescence is illustrated by the data given in Figures 9 and 13. The sign pattern of ΔI vs. λ remains unchanged throughout the pH region 6.5-8.0, but changes slightly at pH >8.0. The CPL signal for Tb^{3+}-L-Ala in solution at pH <6.0 is very weak and g(lum) < 10^{-5} (for the $^7F_5 \leftarrow {}^5D_4$ transition) in this pH region. Over the pH range 6.5-8.0, the values of I and $|\Delta I|$ (at extrema in the total luminescence and CPL spectra) for Tb^{3+}-L-Ala are only about half as large as those observed for Tb^{3+}-L-Ser and only about a sixth as large as these observed for Tb^{3+}-L-Mal. According to arguments given earlier in this discussion, L-Ala should be unidentate throughout the pH region in which Tb^{3+}-L-Ala remains in solution. However, the Tb^{3+}-L-Ala emission/Tb^{3+} emission data displayed in Figure 13, the rather abrupt appearance of observable CPL at pH ~6-7 (CPL is nil below pH 6), and the additional changes in the CPL at pH ~8-9 are difficult to explain without invoking chelate formation through the carboxylate group *and* the α-amino group.

Up to this point we have discussed the emission properties of the Tb^{3+} complexes in terms of structural features characteristic of discrete, mononuclear species. As has been pointed out previously,[13] it is quite possible that under alkaline pH conditions Ln^{3+} ions and carboxylic acids in aqueous solution will tend to form dinuclear or polynuclear type complexes in which either the carboxylate anions or hydroxyl ions (or both) act as bridging groups. If in fact dinuclear and polynuclear species do form in solution and if both Eu^{3+} and Tb^{3+} ions are present, then "mixed" complexes containing both Eu^{3+} and Tb^{3+} should result. For example, under pH conditions in which both carboxyl groups of

L-Mal are deprotonated it is possible that the species [Eu-OOCCH(OH)CH_2COO-Tb]$^{4+}$ could exist. Another possibility is that L-Mal could be terdentate with two of the donor groups attached to Tb^{3+}(Eu^{3+}) and one attached to Eu^{3+}(Tb^{3+}). For ligands such as L-Ala it is possible that "mixed" dinuclear species could be formed by bridging Tb^{3+} and Eu^{3+} through the $-COO^-$ group of the ligand and a OH^- ion from the solution. Generally, in these "mixed" complexes the Eu^{3+} and Tb^{3+} ions will be held in relatively close juxtaposition for relatively long periods of time (that is, long compared with typical lifetimes for "collision complexes" formed between weakly interacting solute species). Under these conditions one might expect significant enhancement of energy transfer processes involving Eu^{3+}-Tb^{3+} pairs.

The energy transfer process, $Tb^{3+}(^5D_4) + Eu^{3+}(^7F_0) \rightarrow Tb^{3+}(^7F_5) + Eu^{3+}(^5D_1)$, purportedly proceeds by an electrostatic dipole-quadrupole mechanism with an approximate "critical transfer distance" of 6.9 Å (in organic glass hosts).[28] In liquid solution (as opposed to solid solution, as a glass), the "critical transfer distance" might be expected to be smaller due to the generally larger number of donor-solvent quenching channels available in liquid solution. Electrostatic dipole-quadrupole interactions are inversely proportional to the eighth power of donor ion-acceptor ion distance. Assuming that enhancement of $Tb^{3+} \rightarrow Eu^{3+}$ energy transfer is directly related to Eu^{3+}-Tb^{3+} "mixed" complex formation, the quenching data plotted in Figures 11-13 can be used to follow dinuclear or polynuclear complex formation as a function of pH. The quenching data for Tb^{3+}-L-Mal-Eu^{3+} suggest that L-Mal may be able to bind both Tb^{3+} and Eu^{3+}, simultaneously, in a pH region where presumably only one carboxyl group is deprotonated. This is possible if both -OH and $-COO^-$ can function as donor groups at pH <3. Recall that the concentration ratios used in the quenching experiments were [Tb^{3+}]/[L-Mal]/[Eu^{3+}] = 1:5:1, so that one would not expect multiple site binding on a single ligand at low pH in the absence of some fairly substantial driving force.

The quenching data for Tb^{3+}-L-Ser-Eu^{3+} suggests weak (or little) multiple site binding (or "mixed" complex formation) in the pH range 2.0-6.5, and strong (or extensive) multiple site binding or "mixed" complex formation at pH > 7.0. In the pH range 2.0-6.5 it is unlikely that dinuclear or polynuclear species could form through OH^- bridging groups; rather, two-site binding (through the -OH and $-COO^-$ moieties of L-Ser) is more likely. At pH >7.0, however, it is possible that Eu^{3+} and Tb^{3+} may be linked through combinations of OH^- and L-Ser bridging groups. There is no evidence of $Tb^{3+} \rightarrow Eu^{3+}$ energy transfer in the Tb^{3+}-L-Ala-Eu^{3+} system until the neutral pH region (where Ln^{3+} hydrolysis begins) is reached and the formation of "mixed" complexes becomes possible via OH^- + L-Ala links between Tb^{3+} and Eu^{3+}. Assuming that the α-NH_2 group is not an effective donor to Ln^{3+} ions in aqueous solution, then L-Ala cannot form "mixed" complexes through multiple site binding.

Unfortunately the quenching data presented in Figures 11-13 do not provide *conclusive* evidence for the formation of "mixed" complexes, or polynuclear, species, as solution pH is increased. It is possible that as solution pH is raised the solvation sphere of Tb^{3+} is altered in such a way that $Tb^{3+} \rightarrow Eu^{3+}$ energy transfer can take place efficiently through the formation of short-lived and weak collision "complexes". The Tb^{3+}-L-Mal-Eu^{3+} quenching data would be difficult to explain on this basis, however. Spectra-structure relationships in chiroptical spectroscopy are not sufficiently developed (especially for the f-f transitions of lanthanon complexes) to permit the direct use of the CPL vs. pH data for resolving the questions of mononuclear vs. di- or polynuclear complex formation, multiple ion binding vs. chelate formation, and OH^- bridged di- or polynuclear complex formation at neutral and/or alkaline pH levels. The CPL reflects rather substantial structural changes taking place as solution pH is changed, but it is not possible to ascertain precisely what these structural changes are.

The data presented in Figures 14 and 15 show that Eu^{3+} ions added to Tb^{3+}-ligand solution quench Tb^{3+} CPL intensity *and* alter the sign pattern of the CPL spectrum in a small, but easily discernible, way. The latter observation suggests that in Tb^{3+}-ligand-Eu^{3+} complexes the chiral nature of the Tb^{3+} binding sites is altered. This could arise from a change in chelation, conformational changes in the ligands, direct interactions between Eu^{3+} and Tb^{3+} ions, or the formation of entirely new coordination systems in the presence of both Tb^{3+} and Eu^{3+} ions.

CPL spectroscopy promises to be a very sensitive probe of molecular stereochemistry and electronic structure. From the present study, it is clear that CPL signatures are much more sensitive to very small or subtle structural alterations than are total emission spectra. Additionally, for chromophores such as the Tb^{3+} and Eu^{3+} ions examined here, CPL is a somewhat more sensitive technique than is CD (with respect to the minimum concentrations of chromophore required to achieve acceptable signal/noise ratios in measuring ΔI or $\Delta\epsilon$). The structural chemistry of Ln^{3+}-carboxylic acid complexes in aqueous solution is exceedingly complex. The methods of study and data presented here do not provide definitive structural characterizations of these systems, but rather contribute information which should be useful in future structural studies of these complex species.

Acknowledgment. We express our gratitude to Professor R. Bruce Martin for his interest in and helpful discussions on the lanthanon chemistry examined in this study, and to Professor James Demas for his advice and aid during the design and construction of the CPL instrumentation. We gratefully acknowledge the financial support provided for this research by the donors of the Petroleum Research Fund, administered by the American Chemical Society, the National Science Foundation, and the Camille and Henry Dreyfus Foundation (through a Teacher-Scholar Award to F.R.).

References and Notes

(1) Address correspondence to this author.
(2) E. R. Birnbaum, J. E. Gomez, and D. W. Darnall, *J. Am. Chem. Soc.*, **92**, 5287 (1970).
(3) D. W. Darnall and E. R. Birnbaum, *J. Biol. Chem.*, **245**, 6484 (1970).
(4) G. E. Smolka, E. R. Birnbaum, and D. W. Darnall, *Biochemistry*, **10**, 4556 (1971).
(5) D. W. Darnall, E. R. Birnbaum, J. E. Gomez, and G. E. Smolka, *Proc. Rare Earth Res. Conf., 9th* **1**, 278 (1971).
(6) K. G. Morallee, E. Nieboer, F. J. Rosolti, R. J. P. Williams, A. V. Xavier, and R. A. Divek, *J. Chem. Soc. D*, 1132 (1970).
(7) C. K. Luk, *Biochemistry*, **10**, 2838 (1971).
(8) A. Gafni and I. Steinberg, *Biochemistry*, **13**, 800 (1974).
(9) H. Donato, Jr., and R. B. Martin, *Biochemistry*, **13**, 4575 (1974).
(10) L. I. Katzin, *Inorg. Chem.*, **7**, 1183 (1968).
(11) L. I. Katzin and E. Gulyas, *Inorg. Chem.*, **7**, 2442 (1968).
(12) L. I. Katzin, *Inorg. Chem.*, **8**, 1649 (1969).
(13) R. Prados, L. G. Stadtherr, H. Donato, and R. B. Martin, *J. Inorg. Nucl. Chem.*, **36**, 689 (1974).
(14) E. R. Birnbaum and D. W. Darnall, *Bioinorg. Chem.*, **3**, 15 (1973).
(15) C. A. Emeis and L. J. Oosterhoff, *Chem. Phys. Lett.*, **1**, 129 (1967).
(16) H. P. J. M. Dekkers, C. A. Emeis, and L. J. Oosterhoff, *J. Am. Chem. Soc.*, **91**, 4589 (1969).
(17) C. A. Emeis and L. J. Oosterhoff, *J. Chem. Phys.*, **54**, 4809 (1971).
(18) A. Gafni and I. Z. Steinberg, *Photochem. Photobiol.*, **15**, 93 (1972).
(19) I. Z. Steinberg and A. Gafni, *Rev. Sci. Instrum.*, **43**, 409 (1972).
(20) J. Schlessinger and I. Steinberg, *Proc. Natl. Acad. Sci. U.S.*, **69**, 769 (1972).
(21) A. Gafni, J. Schlessinger, and I. Z. Steinberg, *Isr. J. Chem.*, **11**, 423 (1973).
(22) C. K. Luk and F. S. Richardson, *Chem. Phys. Lett.*, **25**, 215 (1974).
(23) C. K. Luk and F. S. Richardson, *J. Am. Chem. Soc.*, **96**, 2006 (1974).
(24) J. Snir and J. A. Schellman, *J. Phys. Chem.*, **78**, 387 (1974).

(25) W. T. Carnall, P. R. Fields, and K. Rajnak, *J. Chem. Phys.*, **49**, 4447, 4450 (1968).
(26) C. J. Hawkins, "Absolute Configuration of Metal Complexes", Wiley-Interscience, New York, N.Y., 1971, Chapter 5.
(27) H. F. Halliwell and S. C. Nybrug, *Trans. Faraday Soc.*, **59**, 1126 (1963).
(28) E. Nakazawa and S. Shionoya, *J. Chem. Phys.*, **47**, 3211 (1967).

"Semiempirical" Models for Biomembrane Phase Transitions and Phase Separations

J. A. McCammon* and J. M. Deutch[1]

Contribution from the Department of Chemistry, Harvard University, Cambridge, Massachusetts 02138. *Received March 31, 1975*

Abstract: Experimental studies are reviewed to construct a model for the hydrocarbon chain disordering in "fluid" phospholipid bilayers. Together with approximate expressions for the interactions between neighboring molecules, this information is used to construct a simple statistical thermodynamic theory of the chain "melting" based on the Bragg-Williams approximation. Two unknown parameters in the theory, the interaction between neighboring chains in the "fluid" state and the change in head group interaction associated with the chain "melting", are determined for particular classes of phospholipids by reference to experimental data. The theory is applied to predict the "melting" temperatures of single-component bilayers and the phase diagrams of two-component bilayers. Possible extensions of this type of theory to rationalize other phenomena observed in biological membranes are discussed.

I. Introduction

The thermally induced phase transitions in phospholipid bilayers are known to involve a change in the state of the hydrocarbon chains in the interior of the bilayer. As the temperature is raised, the bilayer is transformed from a highly ordered "solid" state with the chains in all-trans conformations to a more disordered "fluid" state with some gauche rotations in the chain bonds.[4,8]

In dilute, aqueous, lamellar dispersions of highly purified phospholipids, the phase transitions occur at well-defined temperatures which depend on the kind of headgroup and the length and degree of saturation of the hydrocarbon chains.[2,3] In lamellar dispersions of lipid mixtures, the transition occurs over a wider temperature range and is accompanied by the separation of fluid and solid phases of different composition within the bilayer.[4-6] Such transitions have also been observed in cell membranes, where they have a profound effect on cell growth rates.[7] Evidence is accumulating which implicates these transitions in a wide variety of biological control systems, including hormone receptor-enzyme interactions,[8] signal transmission in nerves,[9] enzyme regulation and active transport,[10] and biological clocks.[11] The medical importance of the physical states of membranes and other lipid assemblies has been discussed in several recent articles.[12-16]

Information about the details of the molecular disordering associated with bilayer phase transitions has been provided by recent thermal, spectroscopic, and diffraction studies. In this paper, we use the results of these studies to guide the development of a class of statistical thermodynamic models which describe some aspects of bilayer phase transitions and phase separations. The essential element in these models is the temperature-dependent balance between the energetically preferred solid state, in which the tightly packed all-trans hydrocarbon chains enjoy large van der Waals stabilization, and the high entropy of the fluid state, in which the more loosely packed chains enjoy greater conformational freedom.

In explicitly building experimentally derived structural ideas into our models, we depart from the path of previous theoretical work.[17-21] We sacrifice the elegance of ab initio construction in favor of an approach which should be accessible to a wide audience because of its simplicity and which may be easily modified to encompass a broader range of phenomena. Such statistical thermodynamic models may make possible the practical analysis of data within a simple conceptual scheme, much as helix-coil models have done in the field of protein chemistry.

Although our work is based on well-established bilayer properties where possible, we have had to resort occasionally to rather drastic assumptions where the experimental picture remains cloudy or where cumbersome theoretical refinements seemed premature. These arbitrary elements in this work, which will be discussed later in the paper, should for the most part yield to straightforward corrections with further progress in experiment and theory.

II. Review of Some Experiments

We begin by reviewing briefly some experimental findings, which leads to the simple structural picture upon which our work is based.

A. Unsonicated Lecithin Bilayers. We consider the case of unsonicated lecithin bilayers in which all the hydrocarbon chains are saturated and of a single length. Prolonged sonication produces small vesicles with altered properties[22] which do not necessarily exhibit the phase transition with which we are concerned.[3] Hence, we shall focus almost exclusively on lamellar dispersions in what follows.

Below the phase transition temperatures T_m of such bilayers, X-ray diffraction studies show that the hydrocarbon chains are all-trans and organized in a two-dimensional hexagonal array. The X-ray diffraction pattern indicates that the distance between neighboring chains is 4.8 Å.[23] Proton NMR of these bilayers shows no high-resolution features arising from the hydrocarbon chains.[22] The two chains of a given molecule may not be entirely equivalent; X-ray diffraction studies of the related phosphatidyl ethanolamines show that one chain penetrates more deeply into the bilayer than the other.[24]

As the temperature is raised, calorimetric and volumetric studies show that a broad "pretransition" occurs before the main transition temperature T_m is attained.[3,25] X-Ray dif-